

Control of magnetic relaxation by electric-field-induced ferroelectric phase transition and inhomogeneous domain switching

Tianxiang Nan,¹ Satoru Emori,¹ Bin Peng,² Xinjun Wang,¹ Zhongqiang Hu,¹ Li Xie,¹ Yuan Gao,¹ Hwaider Lin,¹ Jie Jiao,³ Haosu Luo,³ David Budil,⁴ John G. Jones,⁵ Brandon M. Howe,⁵ Gail J. Brown,⁵ Ming Liu,^{2, a)} and Nian Sun^{1, b)}

¹*Department of Electrical and Computer Engineering, Northeastern University, Boston, Massachusetts 02115, USA*

²*Electronic Materials Research Laboratory, Xi'an Jiaotong University, Xi'an 710049, China*

³*Shanghai Institute of Ceramics, Chinese Academy of Sciences, Shanghai 201800, China*

⁴*Department of Chemistry, Northeastern University, Boston, Massachusetts 02115, USA*

⁵*Materials and Manufacturing Directorate, Air Force Research Laboratory, Wright-Patterson AFB, Ohio 45433, USA*

(Dated: June 24, 2021)

Electric-field modulation of magnetism in strain-mediated multiferroic heterostructures is considered a promising scheme for enabling memory and magnetic microwave devices with ultralow power consumption. However, it is not well understood how electric-field-induced strain influences magnetic relaxation, an important physical process for device applications. Here we investigate resonant magnetization dynamics in ferromagnet/ferroelectric multiferroic heterostructures, FeGaB/PMN-PT and NiFe/PMN-PT, in two distinct strain states provided by electric-field-induced ferroelectric phase transition. The strain not only modifies magnetic anisotropy but also magnetic relaxation. In FeGaB/PMN-PT, we observe a nearly two-fold change in intrinsic Gilbert damping by electric field, which is attributed to strain-induced tuning of spin-orbit coupling. By contrast, a small but measurable change in extrinsic linewidth broadening is attributed to inhomogeneous ferroelastic domain switching during the phase transition of the PMN-PT substrate.

^{a)}Electronic mail: mingliu@mail.xjtu.edu.cn

^{b)}Electronic mail: n.sun@neu.edu

Electrical manipulation of the magnetization state is essential for improving the scalability and power efficiency of magnetic random access memory (MRAM)¹⁻⁵. A particularly promising scheme relies on an electric field to assist or induce magnetization switching with minimal power dissipation^{4,6,7}. Multiferroic magnetoelectric materials with coupled magnetization and electric polarization offer possibilities for electric-field-driven magnetization switching at room temperature⁸⁻¹⁴. Such magnetoelectric effects have been demonstrated with strain-¹⁵⁻¹⁹, charge-²⁰⁻²³ and exchange bias mediated coupling mechanisms²⁴⁻²⁷. For example, non-volatile magnetization switching with remarkable modulation of magnetic anisotropy was realized using electric-field-induced piezo-strain at the interface between ferromagnetic and ferroelectric phases²⁸⁻³¹.

On the other hand, a better understanding of the processes responsible for magnetic relaxation, especially at various strain states, is required for electric-field-assisted MRAM or tunable magnetic microwave devices. Recent studies suggest that electric-field-induced changes of magnetic relaxation are correlated to the piezo-strain state or effective magnetic anisotropy³²⁻³⁶. A similar modulation of magnetic relaxation has also been observed in a charge-mediated magnetoelectric heterostructure with ultra-thin ferromagnets³⁷. In general, the contributions to magnetic relaxation include intrinsic Gilbert damping due to spin-orbit coupling and extrinsic linewidth broadening due to inhomogeneity in the ferromagnet. So far, the understanding of how a piezo-strain modifies these intrinsic and extrinsic contributions has been limited³³.

In this work, we quantify electric-field-induced modifications of both intrinsic Gilbert damping and inhomogeneous linewidth broadening in two ferromagnet/ferroelectric heterostructures: $\text{Fe}_7\text{Ga}_2\text{B}_1/\text{Pb}(\text{Mg}_{1/3}\text{Nb}_{2/3})\text{O}_3\text{-PbTiO}_3$ (FeGaB/PMN-PT) with a strong strain-mediated magnetoelectric (magnetostrictive) coupling and $\text{Ni}_{80}\text{Fe}_{20}/\text{Pb}(\text{Mg}_{1/3}\text{Nb}_{2/3})\text{O}_3\text{-PbTiO}_3$ with a negligible magnetoelectric coupling. The rhombohedral (011) oriented PMN-PT substrate provides two distinct strain states through an electric-field-induced phase transformation^{38,39}. We conduct ferromagnetic resonance (FMR) measurements at several applied electric field values to disentangle the intrinsic and extrinsic contributions to magnetic relaxation. FeGaB/PMN-PT exhibits pronounced electric-field-induced modifications of the resonance field and intrinsic Gilbert damping, whereas these parameters remain mostly unchanged for NiFe/PMN-PT. These findings show that magnetic relaxation can be tuned through a strain-mediated modification of spin-orbit coupling in a highly mag-

netostrictive ferromagnet. We also observe in both multiferroic heterostructures a small electric-field-induced change in extrinsic linewidth broadening, which we attribute to the ferroelectric domain state in the PMN-PT substrate.

30-nm thick films of FeGaB and NiFe were sputter-deposited on (011) oriented PMN-PT single crystal substrates buffered with 5-nm thick Ta seed layers. The FeGaB thin film was co-sputtered from Fe₈₀Ga₂₀ (DC sputtered) and B (RF sputtered) targets. Both FeGaB and NiFe films were capped with 2 nm of Al to prevent oxidation. All films were deposited in 3 mTorr Ar atmosphere with a base pressure $\leq 1 \times 10^{-7}$ Torr. The thicknesses of deposited films were calibrated by X-ray reflectivity.

The amorphous FeGaB thin film was selected for its high saturation magnetostriction coefficient of up to 70 ppm⁴⁰ and large magnetoelectric effect when interfaced with ferroelectric materials¹⁹. NiFe was chosen as the control sample with near zero magnetostriction; the thickness of 30 nm is far above the thickness regime that shows high surface magnetostriction⁴¹. Fig. 1 shows magnetic hysteresis loops of FeGaB/PMN-PT and NiFe/PMN-PT, measured by vibrating sample magnetometry with an in-plane magnetic field applied along the [100] direction of PMN-PT. An electric field was applied in the thickness direction of the PMN-PT substrate. Due to the anisotropic piezoelectric coefficient of PMN-PT, an in-plane compressive strain is induced along the [100] direction, which results in uniaxial magnetic anisotropy along the same axis. In FeGaB/PMN-PT the electric field ($E = 8$ kV/cm) increases the saturation field by ≈ 40 mT, whereas only a small change is observed in NiFe/PMN-PT, confirming the significantly different strengths of strain-mediated magnetoelectric coupling for the two multiferroic heterostructures.

Both ferromagnetic thin films exhibit comparatively narrow resonant linewidths, allowing for sensitive detection of the electric-field modification of spin relaxation. Electric-field dependent FMR spectra of FeGaB/PMN-PT and NiFe/PMN-PT were measured using a Bruker EMX electron paramagnetic resonance (EPR) spectrometer with a TE₁₀₂ cavity operated at a microwave frequency of 9.5 GHz. The external magnetic field was applied along the [100] direction of the PMN-PT single crystal. These spectra, shown in Fig. 2(a), (b) were fitted to the derivative of a modified Lorentzian function⁴² to extract the resonance field H_{FMR} and resonance linewidth W . In FeGaB/PMN-PT, upon applying $E = 2$ kV/cm along the thickness direction of PMN-PT, a slight increase of H_{FMR} by 10 mT is observed. A larger shift of 35 mT in H_{FMR} is induced at $E = 8$ kV/cm. In comparison, NiFe/PMN-PT

exhibits a much smaller H_{FMR} shift of 1.5 mT at $E = 8$ kV/cm, as shown in Fig. 2(b).

The shift of H_{FMR} in FeGaB/PMN-PT and NiFe/PMN-PT as a function of E is summarized in Fig. 2(c) and (d). Both samples show hysteric behavior that follows the piezo-strain curve of PMN-PT (inset of Fig. 2(c)) measured with a photonic sensor. This can be understood by the strain-mediated magnetoelectric coupling with the electric-field-induced change of magnetic anisotropy field (ΔH_k) expressed by

$$\Delta H_k = \frac{3\lambda(\sigma_{100} - \sigma_{0-11})}{\mu_0 M_s} \quad (1)$$

where σ_{100} and σ_{0-11} are the in-plane piezo-stress, λ and M_s are the magnetostriction constant and the saturation magnetization respectively. Considering an in-plane compressive strain along the [100] direction and a positive magnetostriction coefficient of both FeGaB and NiFe, a decrease of the magnetic anisotropy field H_k is expected with a positive electric field. The drop of H_k results in an increase of H_{FMR} described by the Kittel equation,

$$f/2\pi = \gamma\mu_0\sqrt{(H_{FMR} + H_k)(H_{FMR} + H_k + M_{eff})} \quad (2)$$

where $\gamma/2\pi=28$ GHz/T and M_{eff} is the effective magnetization. At $E < 4$ kV/cm, H_{FMR} increases linearly, which corresponds to the linear region of piezoelectric effect of PMN-PT with a uniaxial compressive piezo-strain along [100] direction. The sudden change of H_{FMR} at $E = 4$ kV/cm is attributed to the rhombohedral-to-orthorhombic (R-O) phase transition of PMN-PT substrate³⁹. The PMN-PT substrate reverts to the rhombohedral phase upon decreasing the electric field. Therefore, the R-O phase transformation with a large uniaxial in-plane strain induces two stable and reversible magnetic states at $E = 0$ and 8 kV/cm. This provides a reliable platform for studying magnetization dynamics in a controlled manner with the applied electric field.

The peak-to-peak FMR linewidth W of FeGaB/PMN-PT and NiFe/PMN-PT, extracted from the same FMR measurements in Fig. 2, also exhibits a strong dependence on the applied electric field as shown in Fig. 3. For FeGaB/PMN-PT, W remains unchanged within experimental uncertainty at $E < 4$ kV/cm and abruptly increases from ≈ 4.6 mT to ≈ 5.6 mT across the R-O phase transition. By removing the applied electric field, W decreases to the original value with the reversal to the rhombohedral phase. Comparing Fig. 2(c) and 3(a), it is evident that the observed electric-field-induced changes in H_{FMR} and W in FeGaB/PMN-PT are correlated, consistent with recent studies³⁴⁻³⁶. The change

in W indicates a modulation in spin-orbit coupling in the ferromagnet; considering that spin-orbit coupling governs the intrinsic Gilbert damping, it is reasonable that we observe simultaneous modification of W and H_{FMR} by strain in the magnetostrictive FeGaB film.

Given the same sign of the magnetostriction coefficient for FeGaB and NiFe^{40,43}, one would expect to also observe a small increase in W with increasing electric field across the R-O phase transition in NiFe/PMN-PT. However, NiFe/PMN-PT exhibits a decrease in W across the phase transition. This observation indicates that the piezo-strain modifies a different magnetic relaxation contribution in NiFe.

The FMR linewidth W consists of the intrinsic Gilbert damping contribution (parameterized by the damping constant α) and the frequency-independent inhomogeneous linewidth broadening W_0 :

$$W = W_0 + \frac{4\pi\alpha}{\sqrt{3}\gamma} f \quad (3)$$

where f is the microwave excitation frequency. According to Eq. 3, α and W_0 can be determined simply by measuring the frequency dependence of W . For this purpose, we used a home-built broadband FMR system⁴⁴ with a nominal microwave power of -5 dBm and $f = 6-19$ GHz. Just as in the single-frequency measurement using the EPR system (Fig. 2 and Fig. 3), the external magnetic field was applied along the [100] direction of the PMN-PT substrate. By fitting the frequency dependence of H_{FMR} to Eq. 1 (Fig. 4(a), (b)), we obtain anisotropy field shift $\Delta H_k \approx 46$ mT for FeGaB/PMN-PT and $\Delta H_k \approx 1$ mT for NiFe/PMN-PT across the R-O phase transition, in agreement with the single-frequency FMR measurement (Fig. 2), while $\mu_0 M_{eff}$ remains unchanged. Fig. 4(c) and (d) plot W as a function of the frequency for FeGaB/PMN-PT and NiFe/PMN-PT, respectively. From the slope of the linear fit (Eq. 3), we find that α of FeGaB/PMN-PT increases from $(0.6 \pm 0.01) \times 10^{-2}$ at $E = 0$ to $(1.06 \pm 0.02) \times 10^{-2}$ at $E = 8$ kV/cm, whereas α is unchanged at $(1.29 \pm 0.16) \times 10^{-2}$ for NiFe/PMN-PT within experimental uncertainty ($\alpha = (1.27 \pm 0.2) \times 10^{-2}$ at $E = 8$ kV/cm). The large change in α for FeGaB and negligible change for NiFe suggest a strong correlation between magnetostriction and the intrinsic Gilbert damping mechanism. In particular, a large in-plane uniaxial strain generated by the R-O phase transformation induces an additional anisotropy field in FeGaB that enhances the dephasing of the magnetization precession⁴³.

However, both FeGaB/PMN-PT and NiFe/PMN-PT show a decreased W_0 upon applying $E = 8$ kV/cm. This could be related to the ferroelectric domain state in the PMN-PT

substrate that significantly affects the homogeneity of the magnetic film on top. The polarization domain phase images with various applied voltages are shown in Fig. 5 by using a piezo-force microscope. For the unpoled state at, as shown in Fig. 5 (a), the polarization state of PMN-PT surface is inhomogeneous, with polarization vectors oriented randomly along the eight body diagonals of the pseudocubic cell. By applying a voltage of 30 V within the gated area (dashed outline in Fig. 5 (b),(d)), the ferroelectric state becomes saturated within this area with all the polarization vectors pointing upward. This uniformly polarized state alters the surface topology the PMN-PT substrate³¹, thereby reducing the inhomogeneous linewidth broadening W_0 of the ferromagnetic film.

We also measured frequency-dependent FMR spectra with an external magnetic field applied along the $[0\bar{1}1]$ direction to examine the anisotropy of magnetic relaxation. For FeGaB/PMN-PT, α and W_0 are close to the $[100]$ configuration at $E = 0$. At $E = 8$ kV/cm, we observed a non-linear relation between W and f , which might have resulted from a highly non-uniform magnetization state at low fields due to the large electric-field-induced H_k ^{45,46}. To extract α reliably in this case, we would need to conduct FMR measurements at higher frequencies. For NiFe/PMN-PT, α and the electric-field dependence of W_0 are identical for the $[0\bar{1}1]$ and $[100]$ directions. The parameters quantified in this study are summarized in Table I.

In summary, we have quantified electric-field-induced modifications of magnetic anisotropy and magnetic relaxation contributions, namely intrinsic Gilbert damping and inhomogeneous linewidth broadening, in multiferroic heterostructures. A large modification of intrinsic damping arises from strain-induced tuning of spin-orbit coupling in the ferromagnet and is correlated with the magnitude of magnetostriction. A small change in the extrinsic linewidth contribution is attained by controlling the ferroelectric domain states in the substrate. These findings are not only of technology importance for the application on low-power MRAM and magnetic microwave devices, but also permit investigation of the structural dependence of spin-orbit-derived phenomena in magnetic thin films.

Table I. Parameters extracted from broadband FMR at 2 different electric fields

$E(\text{kV/cm})$	FeGaB/PMN-PT		NiFe/PMN-PT	
	0	8	0	8
$4\pi M_{eff}(T)$	1.48 ± 0.01	1.46 ± 0.01	0.96 ± 0.04	0.96 ± 0.04
$H_k(mT)[100]$	5.8 ± 0.5	-41.3 ± 0.3	1.67 ± 0.2	0.27 ± 0.2
$\alpha(10^{-2})[100]$	0.6 ± 0.01	1.06 ± 0.02	1.29 ± 0.16	1.27 ± 0.2
$W_0(mT)[100]$	2.4 ± 0.05	1.8 ± 0.07	0.66 ± 0.06	0.35 ± 0.07
$H_k(mT)[0\bar{1}1]$	3.24 ± 0.4	^a	1.54 ± 0.2	3.1 ± 0.3
$\alpha(10^{-2})[0\bar{1}1]$	0.6 ± 0.02		1.21 ± 0.12	1.29 ± 0.15
$W_0(mT)[0\bar{1}1]$	2.8 ± 0.05		5.9 ± 0.08	2.9 ± 0.05

^a Not able to obtain due to the frequency constraint and the field-dragging effect at measured low frequencies.

This work was supported by the Air Force Research Laboratory through contract FA8650-14-C-5706 and in part by FA8650-14-C-5705, the W.M. Keck Foundation, and the National Natural Science Foundation of China (NSFC) 51328203, 51472199, 11534015.

REFERENCES

- ¹C. Chappert, A. Fert, and F. N. Van Dau, *Nat. Mater.* **6**, 813 (2007).
- ²A. Brataas, A. D. Kent, and H. Ohno, *Nat. Mater.* **11**, 372 (2012).
- ³Y. Shiota, T. Nozaki, F. Bonell, S. Murakami, T. Shinjo, and Y. Suzuki, *Nat. Mater.* **11**, 39 (2012).
- ⁴J.-M. Hu, Z. Li, L.-Q. Chen, and C.-W. Nan, *Nat. Commun.* **2**, 553 (2011).
- ⁵U. Bauer, L. Yao, A. J. Tan, P. Agrawal, S. Emori, H. L. Tuller, S. V. Dijken, and G. S. D. Beach, *Nat. Mater.* **14**, 174 (2014).
- ⁶M. Bibes, *Nature* **7**, 425 (2008).
- ⁷E. Y. Tsymbal, *Nat. Mater.* **11**, 12 (2012).
- ⁸W. Eerenstein, N. D. Mathur, and J. F. Scott, *Nature* **442**, 759 (2006).
- ⁹M. Fiebig, *J. Phys. D. Appl. Phys.* **38**, R123 (2005).
- ¹⁰R. Ramesh and N. a. Spaldin, *Nat. Mater.* **6**, 21 (2007).
- ¹¹J. Ma, J. Hu, Z. Li, and C. W. Nan, *Adv. Mater.* **23**, 1062 (2011).
- ¹²N. X. Sun and G. Srinivasan, *Spin* **2**, 1240004 (2012).
- ¹³C. a. F. Vaz, *J. Phys. Condens. Matter* **24**, 333201 (2012).
- ¹⁴S. Fusil, V. Garcia, a. Barthélémy, and M. Bibes, *Annu. Rev. Mater. Res.* **44**, 91 (2014).
- ¹⁵C. W. Nan, *Phys. Rev. B* **50**, 6082 (1994).
- ¹⁶G. Srinivasan, E. Rasmussen, J. Gallegos, R. Srinivasan, Y. Bokhan, and V. Laletin, *Phys. Rev. B* **64**, 214408 (2002).
- ¹⁷C. Thiele, K. Dörr, O. Bilani, J. Rödel, and L. Schultz, *Phys. Rev. B* **75**, 054408 (2007).
- ¹⁸Y. Jia, H. Luo, X. Zhao, and F. Wang, *Adv. Mater.* **20**, 4776 (2008).
- ¹⁹J. Lou, M. Liu, D. Reed, Y. Ren, and N. X. Sun, *Adv. Mater.* **21**, 4711 (2009).
- ²⁰M. Weisheit, S. Fähler, A. Marty, Y. Souche, C. Poinsignon, and D. Givord, *Science* **315**, 349 (2007).
- ²¹T. Maruyama, Y. Shiota, T. Nozaki, K. Ohta, N. Toda, M. Mizuguchi, a. a. Tulapurkar, T. Shinjo, M. Shiraishi, S. Mizukami, Y. Ando, and Y. Suzuki, *Nat. Nanotechnol.* **4**, 158 (2009).
- ²²W.-G. Wang, M. Li, S. Hageman, and C. L. Chien, *Nat. Mater.* **11**, 64 (2012).
- ²³Z. Zhou, T. X. Nan, Y. Gao, X. Yang, S. Beguhn, M. Li, Y. Lu, J. L. Wang, M. Liu, K. Mahalingam, B. M. Howe, G. J. Brown, and N. X. Sun, *Appl. Phys. Lett.* **103**, 232906

- (2013).
- ²⁴S. H. Baek, H. W. Jang, C. M. Folkman, Y. L. Li, B. Winchester, J. X. Zhang, Q. He, Y. H. Chu, C. T. Nelson, M. S. Rzechowski, X. Q. Pan, R. Ramesh, L. Q. Chen, and C. B. Eom, *Nat. Mater.* **9**, 309 (2010).
- ²⁵J. T. Heron, M. Trassin, K. Ashraf, M. Gajek, Q. He, S. Y. Yang, D. E. Nikonov, Y. H. Chu, S. Salahuddin, and R. Ramesh, *Phys. Rev. Lett.* **107**, 217202 (2011).
- ²⁶J. T. Heron, J. L. Bosse, Q. He, Y. Gao, M. Trassin, L. Ye, J. D. Clarkson, C. Wang, J. Liu, S. Salahuddin, D. C. Ralph, D. G. Schlom, J. Íñiguez, B. D. Huey, and R. Ramesh, *Nature* **516**, 370 (2014).
- ²⁷Z. Zhou, M. Trassin, Y. Gao, Y. Gao, D. Qiu, K. Ashraf, T. Nan, X. Yang, S. R. Bowden, D. T. Pierce, M. D. Stiles, J. Unguris, M. Liu, B. M. Howe, G. J. Brown, S. Salahuddin, R. Ramesh, and N. X. Sun, *Nat. Commun.* **6**, 6082 (2015).
- ²⁸T. Wu, A. Bur, P. Zhao, K. P. Mohanchandra, K. Wong, K. L. Wang, C. S. Lynch, and G. P. Carman, *Appl. Phys. Lett.* **98**, 012504 (2011).
- ²⁹S. Zhang, Y. G. Zhao, P. S. Li, J. J. Yang, S. Rizwan, J. X. Zhang, J. Seidel, T. L. Qu, Y. J. Yang, Z. L. Luo, Q. He, T. Zou, Q. P. Chen, J. W. Wang, L. F. Yang, Y. Sun, Y. Z. Wu, X. Xiao, X. F. Jin, J. Huang, C. Gao, X. F. Han, and R. Ramesh, *Phys. Rev. Lett.* **108**, 137203 (2012).
- ³⁰T. X. Nan, Z. Y. Zhou, J. Lou, M. Liu, X. Yang, Y. Gao, S. Rand, and N. X. Sun, *Appl. Phys. Lett.* **100**, 132409 (2012).
- ³¹M. Liu, B. M. Howe, L. Grazulis, K. Mahalingam, T. Nan, N. X. Sun, and G. J. Brown, *Adv. Mater.* **25**, 4886 (2013).
- ³²J. Lou, D. Reed, C. Pettiford, M. Liu, P. Han, S. Dong, and N. X. Sun, *Appl. Phys. Lett.* **92**, 262502 (2008).
- ³³H. Zhou, X. Fan, F. Wang, C. Jiang, J. Rao, X. Zhao, Y. S. Gui, C. M. Hu, and D. Xue, *Appl. Phys. Lett.* **104**, 102401 (2014).
- ³⁴F. Zighem, M. Belmeguenai, D. Faurie, H. Haddadi, and J. Moulin, *Rev. Sci. Instrum.* **85**, 103905 (2014).
- ³⁵S. Li, Q. Xue, J.-G. Duh, H. Du, J. Xu, Y. Wan, Q. Li, and Y. Lü, *Sci. Rep.* **4**, 7393 (2014).
- ³⁶G. Yu, Z. Wang, M. Abolfath-Beygi, C. He, X. Li, K. L. Wong, P. Nordeen, H. Wu, G. P. Carman, X. Han, I. a. Alhomoudi, P. K. Amiri, and K. L. Wang, *Appl. Phys. Lett.* **106**,

072402 (2015).

- ³⁷A. Okada, S. Kanai, M. Yamanouchi, S. Ikeda, F. Matsukura, and H. Ohno, *Appl. Phys. Lett.* **105**, 052415 (2014).
- ³⁸M. Shanthi and L. C. Lim, *Appl. Phys. Lett.* **95**, 102901 (2009).
- ³⁹F. Li, S. Zhang, D. Lin, J. Luo, Z. Xu, X. Wei, and T. R. ShROUT, *J. Appl. Phys.* **109**, 14108 (2011).
- ⁴⁰J. Lou, R. E. Insignares, Z. Cai, K. S. Ziemer, M. Liu, and N. X. Sun, *Appl. Phys. Lett.* **91**, 182504 (2007).
- ⁴¹O. Song, C. a. Ballentine, and R. C. O’Handley, *Appl. Phys. Lett.* **64**, 2593 (1994).
- ⁴²A. L. Stancik and E. B. Brauns, *Vib. Spectrosc.* **47**, 66 (2008).
- ⁴³R. Bonin, M. L. Schneider, T. J. Silva, and J. P. Nibarger, *J. Appl. Phys.* **98**, 123904 (2005).
- ⁴⁴S. Beguhn, Z. Zhou, S. Rand, X. Yang, J. Lou, and N. X. Sun, *J. Appl. Phys.* **111**, 07A503 (2012).
- ⁴⁵G. Woltersdorf and B. Heinrich, *Phys. Rev. B* **69**, 184417 (2004).
- ⁴⁶K. Zakeri, J. Lindner, I. Barsukov, R. Meckenstock, M. Farle, U. Von Hörsten, H. Wende, W. Keune, J. Rocker, S. S. Kalarickal, K. Lenz, W. Kuch, K. Baberschke, and Z. Frait, *Phys. Rev. B* **76**, 104416 (2007).

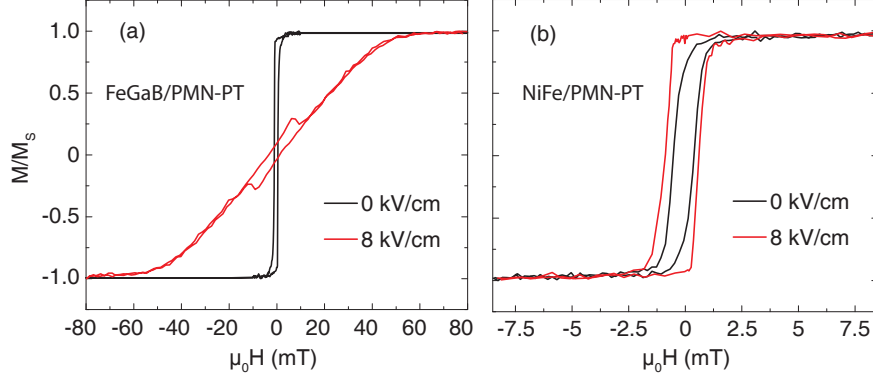


Figure 1. (a,b) Electric-field dependent magnetic hysteresis loops with the magnetic field applied along the [100] direction for FeGaB/PMN-PT (a) and NiFe/PMN-PT (b).

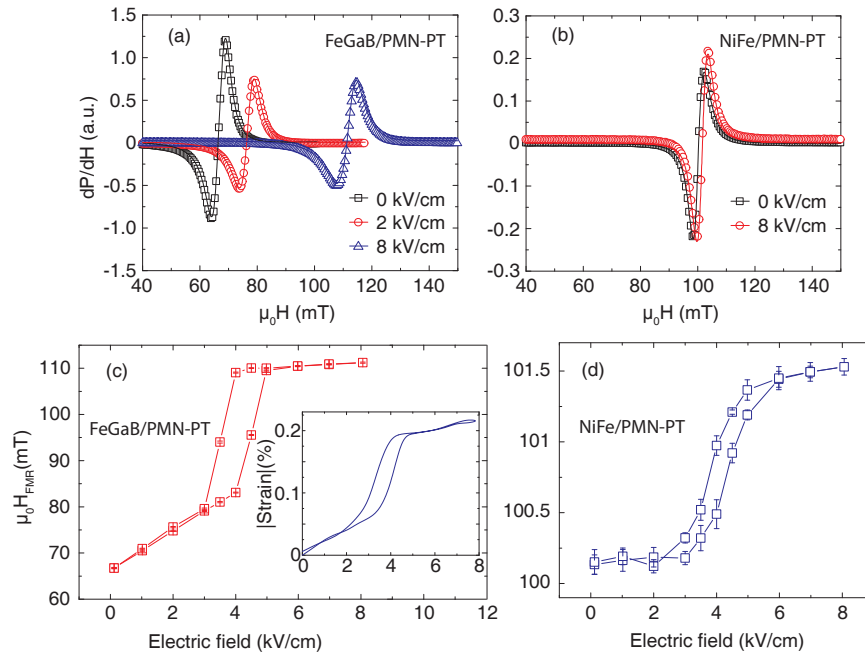


Figure 2. (a,b) FMR (fixed at 9.5 GHz) spectra at various electric fields with the magnetic field applied along the [100] direction for FeGaB/PMN-PT (a) and NiFe/PMN-PT (b). (c,d) Resonance field HFMR as a function of the applied electric field for FeGaB/PMN-PT (a) and NiFe/PMN-PT (b). Inset of (c) shows the piezo-strain as a function of electric field for PMN-PT substrate along the [100] direction.

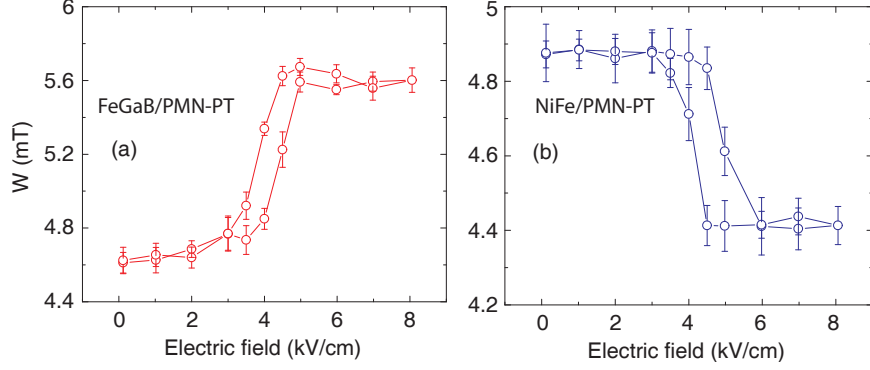


Figure 3. (a,b) Resonance linewidth W at 9.5 GHz with the magnetic field applied along the [100] direction as a function of the applied electric field for FeGaB/PMN-PT (a) and NiFe/PMN-PT (b).

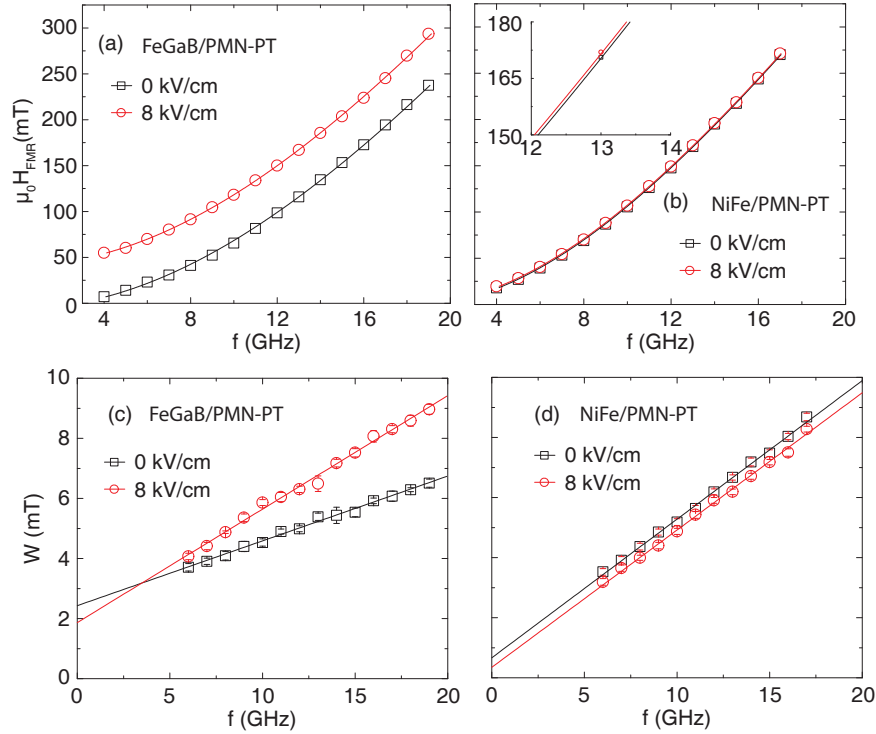


Figure 4. (a,b) Frequency f as a function of resonance field H_{FMR} at different electric fields for FeGaB/PMN-PT (a) and NiFe/PMN-PT (b). (c,d) Linewidth W as a function of frequency f at different electric fields for FeGaB/PMN-PT (c) and NiFe/PMN-PT (d). The magnetic field was applied along the [100] direction.

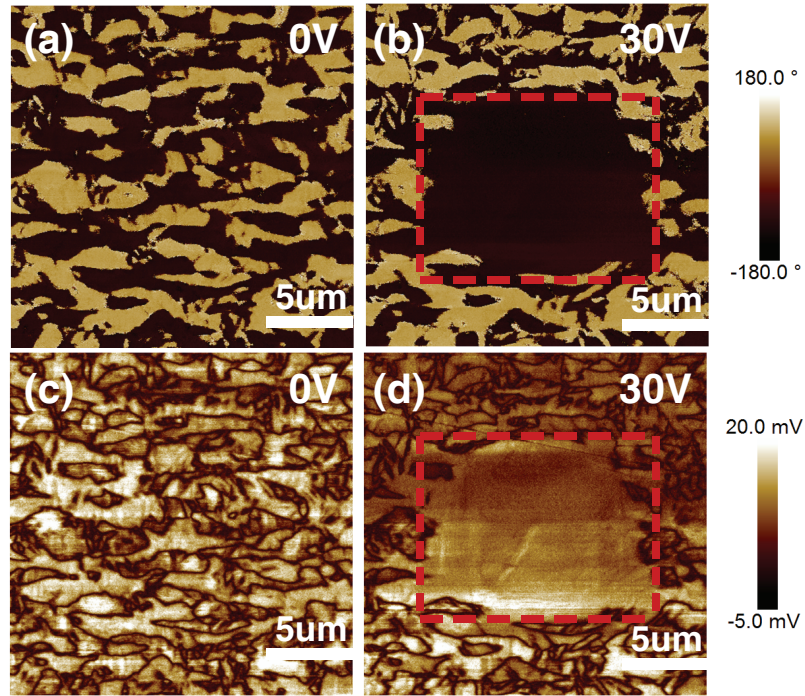


Figure 5. (a,b) The out-of-plane vertical PFM (VPFM) phase images upon applying different voltages to the square area outlined by a red dashed line. (c,d) Corresponding amplitude images at different voltage biases.